

# Predicting Nuclear Resonance Vibrational Spectra of [Fe(OEP)(NO)]

Qian Peng,<sup>†</sup> Jeffrey W. Pavlik,<sup>†</sup> W. Robert Scheidt,<sup>†</sup> and Olaf Wiest<sup>†,‡,\*</sup>

<sup>†</sup>Department of Chemistry and Biochemistry, University of Notre Dame, Notre Dame, Indiana 46556, United States

<sup>‡</sup>School of Chemical Biology and Biotechnology, Peking University, Shenzhen Graduate School, Shenzhen 518055, China

 Supporting Information

**ABSTRACT:** Nuclear resonance vibrational spectroscopy (NRVS) is a sensitive vibrational probe for biologically important heme complexes. The exquisite sensitivity of the NRVS data to the electronic structure provides detailed insights into the nature of these interesting compounds but requires highly accurate computational methods for the mode assignments. To determine the best combinations of density functionals and basis sets, a series of benchmark DFT calculations on the previously characterized complex [Fe(OEP)NO] ( $OEP^{2-}$  = octaethylporphyrinato dianion) was performed. A test set of 21 methodology combinations including eight functionals (BP86, mPWPW91, B3LYP, PBE1PBE, M062X, M06L, LC-BP86, and  $\omega$ B97X-D) and five basis set (VTZ, TZVP, and LanL2DZ for iron and 6-31G\* and 6-31+G\* for other atoms) was carried out to calculate electronic structures and vibrational frequencies. We also implemented the conversion of frequency calculations into orientation-selective mode composition factors ( $e^2$ ), which can be used to simulate the vibrational density of states (VDOS) using Gaussian normal distribution functions. These use a series of user-friendly scripts for their application to NRVS. The structures as well as the isotropic and anisotropic NRVS of [Fe(OEP)NO] obtained with the M06L functional with a variety of basis sets are found to best reproduce the available experimental data, followed by B3LYP/LanL2DZ calculations. Other density functionals and basis sets do not produce the same level of accuracy. The noticeably worse agreement between theory and experiment for the out-of-plane NRVS compared with the excellent performance of the M06L functional for the in-plane prediction is attributed to deficiencies of the physical model rather than the computational methodology.

## INTRODUCTION

Iron porphyrinates<sup>1</sup> are among the most important biological prosthetic groups and occur in many proteins and enzymes. A pivotal property of iron porphyrinates is the strong attraction of the central iron to axial ligands including histidine and diatomics like O<sub>2</sub> in hemoglobin (Hb) and myoglobin (Mb). The binding and dissociation reactions of small ligands like O<sub>2</sub> and NO in heme proteins are important biological processes.<sup>2</sup> In nature, NO is discriminated from O<sub>2</sub> quite efficiently, presumably due to conformational changes in the protein imparted upon ligand binding.<sup>3</sup> Infrared and resonance Raman spectroscopy have provided insights into the interplay of structure and function of heme active sites.<sup>4</sup> However, these techniques have some inherent limitations, especially in the low frequency regime where mode assignment is hampered by weak signals, spectral congestion, and low sensitivity to isotopic substitution.<sup>5</sup> Nuclear resonance vibrational spectroscopy<sup>6</sup> (NRVS) provides much higher selectivity because only the vibrational modes of the probe nucleus (<sup>57</sup>Fe in the case of iron porphyrinates) contribute to the observed signal. Moreover, the NRVS intensity is directly related to the magnitude and direction of the motion; hence the method has a unique quantitative component in the measured vibrational spectrum. This method has been applied to heme enzymes, nitrogenase, and model complexes.<sup>7</sup> However, the spectral crowding in the NRVS response region makes the spectra hard to identify for several vibrational modes, even for some very significant modes. In these cases, the computational prediction of NRVS spectra and comparison with experiment is an invaluable and indispensable tool in the assignment of the

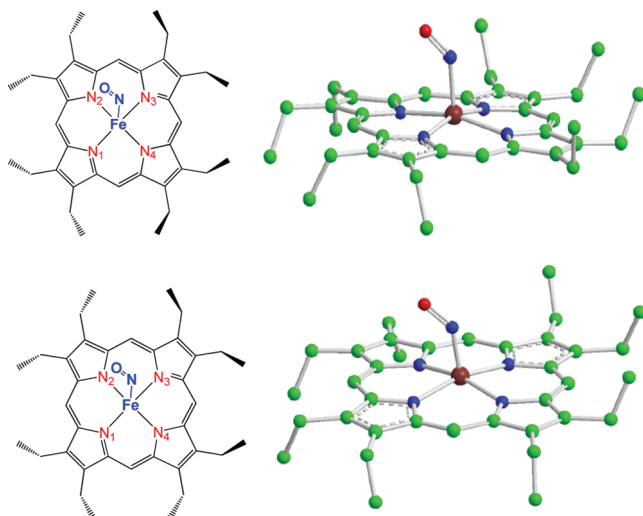
observed modes. In turn, good agreement between experimental and computed NRVS spectra validates the computed results and increases the confidence in an analysis of the geometric and electronic structure of the entire molecule.

Density functional theory (DFT) methods now predict electronic structures and properties for molecules of increasing sizes, including detailed descriptions of their vibrational dynamics.<sup>8</sup> Very recently, Noddleman and co-workers used a series of well-established density functionals to accurately calibrate the <sup>57</sup>Fe Mössbauer isomer shift and quadrupole splitting parameters.<sup>8d</sup> Despite the complex electronic structure of heme complexes, DFT calculations are becoming increasingly accurate in the prediction of vibrational frequencies and are a very useful tool in mode assignments. The new generation of recently developed density functionals (such as the M0X series that address some of the shortcomings of previous DFT methods) holds significant promise for clarifying the character of a vibronic mode. The rich data set of vibrational frequencies, amplitudes, and directions available from NRVS can also provide a particularly rigorous test of the ability of DFT calculations to predict the vibrational dynamics of transition metal complexes.<sup>9</sup>

Lehnert and co-workers developed a useful method called “quantum chemistry centered normal coordinate analysis” (QCC-NCA)<sup>10</sup> to fit some of the important NRVS peaks (bending and stretch modes) based on initial normal frequency calculations from Gaussian software. Clearly, a more rigorous and direct use of the

**Received:** September 15, 2011

**Published:** November 29, 2011

**Scheme 1.** Conformations of [Fe(OEP)(NO)]

normal modes would be preferable over such fitting procedures. In addition, the DFT methods applied to the prediction of NRVS have so far been limited to BP86 and B3LYP functionals, which do not describe dispersive interactions and suffer for incorrect descriptions of the self-interaction, especially in open shell systems.<sup>11</sup> As a result, they do not always have good agreement with experimental observations.<sup>5,12</sup> To the best of our knowledge, there have been no systematic studies of more modern functionals that provide a much more balanced description of the electronic structure.

In this paper, we report a series of computational studies at different levels of theory, including the modern functionals that have not previously been tested for this purpose, with the goal of establishing best practices for the prediction and interpretation of NRVS data. Specifically, we compare the performance of different computational methods for (1) structure predictions, (2) the Fe–NO stretch and Fe–N–O bending vibrational modes, (3) the prediction of NRVS, and (4) directional NRVS (in-plane and out-of-plane). Finally, we discuss the effects of model issues. We also describe a set of user-friendly scripts that allow the direct conversion of frequency calculations into orientation-selective NRVS plots that can directly be compared to experimental data.

These calculations were benchmarked for [Fe(OEP)(NO)], a model complex for biologically relevant interactions of nitric oxide and heme iron for which there are high-resolution structures and NRVS data available. The rich data set of vibrational frequencies and directions available from NRVS for [Fe(OEP)(NO)] can provide a highly reliable test for our evaluation of DFT functionals and basis sets. At the same time, [Fe(OEP)(NO)] is a challenging molecule for DFT calculations because of the well-known difficulty in treating unpaired  $S = 1/2$  spin systems.<sup>13</sup> [Fe(OEP)NO] can adopt two conformations with different ethyl orientations in the solid state.<sup>14</sup> One conformation is from a triclinic crystal that has four neighboring ethyl groups of OEP pointing to one face of the porphyrin, whereas the remaining four ethyl groups are in the opposite direction (Scheme 1, top). The other conformation is from a monoclinic crystal with five and three ethyl groups of OEP pointing to each face of the porphyrin plane (Scheme 1, bottom).

Ferrous heme-nitrosyls have low energy barriers for rotations of the NO ligand around the Fe–NO bond,<sup>15</sup> which causes disorder in the NO orientation.<sup>16</sup> The recent work by Lehnert

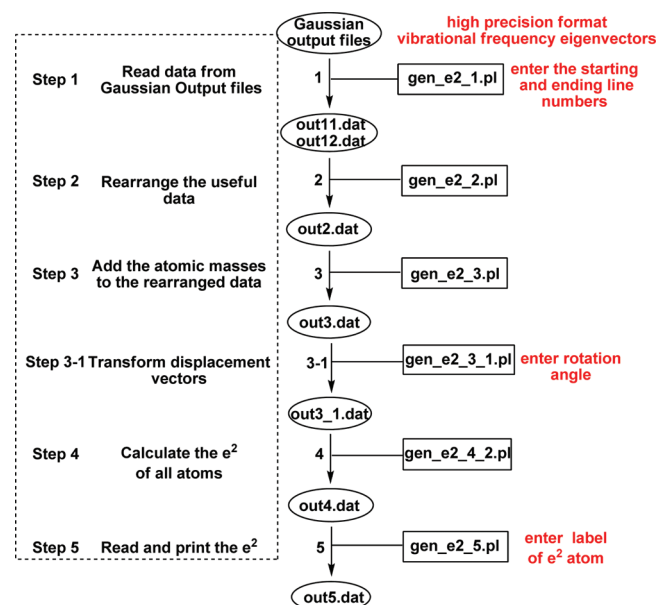


**Figure 1.** Flowchart of the scripts that generate  $e^2$  in different orientations. The rectangles and ovals represent the script files and output files in every step, respectively.

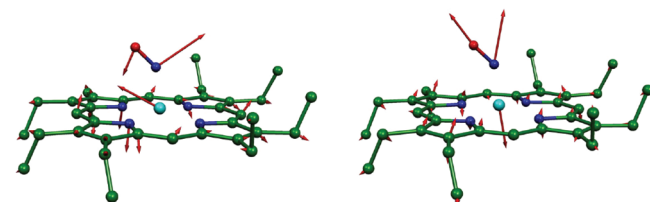


**Figure 2.** Fe–N–O bending (left) and Fe–NO stretch (right) vibrational modes. Hydrogen atoms and Fe–N bonds have been omitted for clarity. The vector is shown  $100(m_j/m_{Fe})^{1/2}$  times longer than the zero-point vibrational amplitude of atom  $j$ .

and co-workers used B3LYP/LanL2DZ and BP86/LanL2DZ\* calculations to test the 12 possible conformations for the disordered NO and rotated ethyl substituents of [Fe(OEP)(NO)].<sup>10d</sup> Their prediction of NRVS spectra followed by QCC-NCA fitting has shown fair agreement with their powder measurements. However, comparisons of DFT predictions to powder measurements are lacking in the directional character of modes. We previously completed single-crystal measurements on [Fe(OEP)(NO)], taken at three orthogonal crystallographic directions, which shows significant directional anisotropy.<sup>12b</sup> In contrast to typical nitrosyl iron porphyrins, [Fe(OEP)(NO)] exhibits a completely ordered NO group and is ideal for the oriented single-crystal NRVS experiment and for DFT calculations.

## METHODS

**Electronic Structure Calculations.** The G09 program package<sup>17</sup> was used to optimize the structures and for frequency analysis in our study. The model complex [Fe(OEP)(NO)] ( $S = 1/2$ ) was fully optimized without any constraints using the spin unrestricted DFT method. The starting structure was obtained from the crystal structure of triclinic [Fe(OEP)(NO)].<sup>14</sup> Frequency calculations were performed on the fully optimized structures at the

**Table 1.** Observed and Calculated Geometric Parameters of [Fe(OEP)(NO)]<sup>a</sup>

[Fe(OEP)(NO)]		geometric parameters (pm or degree)									
functional	basis set	Fe–NO	$\Delta_{\text{Fe}-\text{NO}}$	N–O	$\Delta_{\text{N}-\text{O}}$	$\angle \text{Fe}-\text{N}-\text{O}$	$\Delta_{\angle \text{Fe}-\text{N}-\text{O}}$	$\text{Fe}-\text{N}_{\text{short}}^{\text{c}}$	$\text{Fe}-\text{N}_{\text{long}}^{\text{c}}$	$\Delta_{\text{long}-\text{short}}$	ref
triclinic crystal (experimental)		173.1		116.8		142.7		199.9	202.0	2.1	12b
BP86	6-31G*/VTZ	169.7	-3.4	119.2	2.4	143.2	0.5	200.3	203.1	2.8	12b
	6-31+G*(N,O) <sup>b</sup> /VTZ	169.6	-3.5	119.5	2.7	143.6	0.9	200.3	203.3	3.0	f
	6-31G*/TZVP	169.6	-3.5	119.1	2.3	144.9	2.2	200.9	203.9	3.0	f
MPWPW91	6-31G*/VTZ	169.8	-3.3	119.0	2.2	142.8	0.1	200.1	202.9	2.8	f
	6-31+G*(N,O) <sup>b</sup> /VTZ	169.6	-3.5	119.3	2.5	143.7	1.0	200.3	203.3	3.0	f
	6-31G*/TZVP	169.6	-3.5	118.9	2.1	144.7	2.0	200.8	203.8	3.0	f
B3LYP <sup>d</sup>	6-31G*/Lanl2DZ	172.8	-0.3	117.0	0.2	139.8	-2.9	200.7	203.1	2.4	f
	Lanl2DZ <sup>c</sup>	174.2	1.1	121.5	4.7	142.9	0.2	201.3	202.7	1.4	10d <sup>g</sup>
PBE1PBE	6-31G*/VTZ	170.7	-2.4	116.5	-0.3	140.2	-2.5	199.2	201.3	2.1	f
M062X <sup>d</sup>	Lanl2DZ	231.1	58	118.2	1.4	125.8	-16.9	203.0	202.0	-1.0	f
M06L	6-31G*/VTZ	172.2	-0.9	118.0	1.2	140.2	-2.5	200.6	202.6	2.0	f
	6-31+G*(N,O) <sup>b</sup> /VTZ	172.4	-0.7	118.1	1.3	140.7	-2.0	200.8	203.1	2.3	f
	6-31G*/TZVP	172.0	-1.1	117.9	1.1	141.5	-1.2	201.1	203.2	2.1	f
	6-31+G*(N,O) <sup>b</sup> /TZVP	172.4	-0.7	118.1	1.3	140.9	-1.8	201.1	203.3	2.2	f
	6-31G*/Lanl2DZ	172.2	-0.9	117.8	1.0	140.2	-2.5	200.2	202.7	2.5	f
LC-BP86	Lanl2DZ <sup>c</sup>	173.5	0.4	121.9	5.1	141.9	-0.8	200.6	202.5	1.9	f
	6-31G*/VTZ	170.9	-2.2	115.2	-1.6	139.1	-3.6	196.1	197.5	1.4	f
$\omega$ B97X-D	6-31G*/VTZ	172.6	-0.5	116.5	-0.3	139.3	-3.4	199.8	201.2	1.4	f
	6-31+G*(N,O) <sup>b</sup> /VTZ	172.3	-0.8	116.6	-0.2	139.7	-3.0	199.9	201.5	1.6	f

<sup>a</sup> Basis sets: 6-31G\* for H, C, N and O; VTZ, TZVP, or Lanl2DZ for Fe. <sup>b</sup> Basis set: 6-31G\* for H and C, 6-31+G\* for N and O. <sup>c</sup> Basis set Lanl2DZ for all of the atoms. <sup>d</sup> Basis set VTZ; TZVP for Fe is also applied but failed to obtain the converged wave functions. <sup>e</sup> Values for Fe–N<sub>short</sub> and Fe–N<sub>long</sub> (N<sub>short</sub> = the average of two short Fe and porphyrin N atom, N<sub>long</sub> = the average of two long Fe and porphyrin N atom; Δ<sub>long–short</sub> is the difference between the experimental data and calculation with corresponding bond lengths and angles. <sup>f</sup> This work. <sup>g</sup> Only isotropic terms; for anisotropic terms, see this work.

same basis level to obtain the vibrational frequencies with the <sup>57</sup>Fe isotope set, which can yield inelastic scattering at the 14.4125 keV nuclear resonance line in the NRVS experiment.<sup>18</sup> It is well-known that the frequencies obtained from harmonic frequency analyses are larger than the experimentally observed values due to the neglect of anharmonicity.<sup>19</sup> This is typically addressed using scaling factors. However, the precise values are not only method and basis set dependent but are also different for different frequency regimes and have been validated mostly for pure organic molecules rather than the metal complexes discussed here. Therefore, the choice of the precise value would be ambiguous, and the frequencies reported here were not scaled. The frequency output data have been created using the high precision format vibrational frequency eigenvectors in order to calculate mode composition factors ( $e^2$ ) and vibrational densities of state (VDOS) as described below.

We studied five classes of functionals: (1) generalized gradient approximation (GGA) functionals (BP86,<sup>20</sup> mPW91<sup>21</sup>) which contain the exchange and GGA correlation functionals.; (2) hybrid-GGA functionals (B3LYP,<sup>22</sup> PBE1PBE<sup>23</sup>), which contain a mixture of Hartree–Fock exchange with DFT exchange-correlation; (3) hybrid meta-GGA functionals (M062X<sup>24</sup>); (4) meta-GGA functionals (M06L<sup>25</sup>), M06L being a local meta-GGA functional; and (5) long-range GGA functionals (LC-BP86,<sup>20,26</sup>  $\omega$ B97X-D<sup>27</sup>) which contain long-range corrections. These were combined with different basis sets<sup>28</sup> as specified in the Results section. In general, we used triple- $\zeta$  valence basis sets with (TZVP) or without (VTZ) polarization functions or a double  $\zeta$  effective core potential (Lanl2DZ) on iron and 6-31G\* or 6-31+G\* basis sets for all other atoms. In order to allow comparison to Lehnert's results,<sup>10d</sup> the Lanl2DZ basis set was also tested for all atoms.

**Calculation of the NRVS Data.** The first step in the calculation of the NRVS data is the calculation of the predicted mode composition factors, which are based on the atomic displacements of each atom ( $r_i$ ) from the analytical frequency analysis using DFT. The mode composition factors  $e_{ja}^2$ , which represent the fraction of the kinetic energy in frequency mode  $\alpha$  due to the motion of atom  $j$  ( $j = {^{57}\text{Fe}}$  for NRVS), provide a convenient quantitative comparison between measurements and calculations.<sup>29</sup> Mode composition factors are defined in eq 1:

$$e_{ja}^2 = \frac{m_j r_j^2}{\sum m_i r_i^2} \quad (1)$$

where  $m_i$  is the atomic mass of atom  $i$  and  $r_i$  is the absolute length of the Cartesian displacement vector for atom  $i$  in Ångströms. The mode composition factors for different directions are defined in terms of an averaged porphyrin plane as in-plane, which can be calculated from a projection of the atomic displacement vector  $x$  and  $y$  (eq 2). The out-of-plane atomic displacement perpendicular to the resulting porphyrin plane for a normal mode is obtained from a projection of the atomic displacement vector  $z$  (eq 3).

$$e_{ja, \text{in-plane}}^2 = \frac{m_j (r_{jx}^2 + r_{jy}^2)}{\sum m_i r_i^2} \quad (2)$$

$$e_{ja, \text{out-plane}}^2 = \frac{m_j r_{jz}^2}{\sum m_i r_i^2} \quad (3)$$

The Perl scripts to calculate the mode composition factors are provided in the Supporting Information and directly read from a

**Table 2.** Observed and Calculated Vibrations of [Fe(OEP)(NO)]<sup>a</sup>

[Fe(OEP)(NO)]		vibrational frequencies (cm <sup>-1</sup> )			
functional	basis set	$\nu$ (Fe–NO)	$\delta$ (Fe–N–O)	$\nu$ (N–O)	ref
triclinic crystal (experimental)		517	393	1673	12b
BP86	6-31G*/VTZ	623	417	1719	12b
	6-31+G*(N,O) <sup>b</sup> /VTZ	617	415	1689	e
	6-31G*/TZVP	618	410	1730	e
MPWPW91	6-31G*/VTZ	621	419	1727	e
	6-31+G*(N,O) <sup>b</sup> /VTZ	615	415	1698	e
	6-31G*/TZVP	616	410	1739	e
B3LYP <sup>d</sup>	6-31G*/Lanl2DZ	517/521	417	1828	e
	Lanl2DZ <sup>c</sup>	498/504	407	1616	10d <sup>f</sup>
PBE1PBE	6-31G*/VTZ	547	433	1885	e
M062X <sup>d</sup>	Lanl2DZ				e
M06L	6-31G*/VTZ	494/499	396	1798	e
	6-31+G*(N,O) <sup>b</sup> /VTZ	477/485	391	1779	e
	6-31G*/TZVP	495/500	388	1807	e
	6-31+G*(N,O) <sup>b</sup> /TZVP	477/485	386	1782	e
	6-31G*/Lanl2DZ	517	405	1804	e
	Lanl2DZ <sup>c</sup>	448	401	1624	e
LC-BP86	6-31G*/VTZ	551	443	2001	e
$\omega$ B97X-D	6-31G*/VTZ	532	425	1891	e
	6-31+G*(N,O) <sup>b</sup> /VTZ	522	422	1865	e

<sup>a</sup> Basis sets: 6-31G\* for H, C, N, and O; VTZ, TZVP, or Lanl2DZ for Fe. <sup>b</sup> Basis set: 6-31G\* for H and C, 6-31+G\* for N and O. <sup>c</sup> Basis set Lanl2DZ for all of the atoms. <sup>d</sup> Basis set VTZ; TZVP for Fe is also applied but failed to obtain the converged wave functions. <sup>e</sup> This work. <sup>f</sup> Only isotropic terms; for anisotropic terms, see this work.

G09 frequency output file using a high precision format for the vibrational frequency eigenvectors. Figure 1 showed the flow scheme for the scripts calculating  $e_{ja}^2$ . The total procedures include six simple scripts, three of which (shown in red in Figure 1) need user input based on the specific molecule to be studied. In step 1, the starting and ending line numbers are needed for the frequency range of interest. In our case, a frequency range of 0–800 cm<sup>-1</sup> is defined to follow the range of NRVS in the experimental observations. In step 3-1, the orientation of interest is set as shown in Scheme 2. For porphyrins, the standard orientation used in G09 aligns the *x* and *y* coordinates along the iron–meso-carbon axes (4C-inplane), but the stretch vibration along the iron–nitrogen bond (4N-inplane) is needed. Thus, the calculation of  $e_{ja}^2$  requires in some cases a rotation of the coordinates by 45°. In the final step, the desired  $e^2$  data (in our case for <sup>57</sup>Fe, but available for any set of atoms) is read out.

The predicted mode composition factors  $e_{ja}^2$  can also be compared to the integrated spectral areas obtained from NRVS.<sup>5</sup> Therefore, vibrational densities of state (VDOS) intensities can be simulated from the mode composition factors using the Gaussian normal distributions function, where the full width at half height (fwhh) is defined appropriately by considering the spectral resolution in the experiment. In this study, the MATLAB R2010a software was used to generate the predicted NRVS curves.

## ■ RESULTS AND DISCUSSION

**Effects of DFT Method and Basis Set on the Calculated Geometry of [Fe(OEP)(NO)].** To investigate the effects of the DFT method and basis sets, we have performed DFT calculations on [Fe(OEP)(NO)] applying the functionals and basis sets discussed above. Tables 1 and 2 show the selected geometric and

vibrational properties of [Fe(OEP)(NO)] with the different basis sets in each density functional. In general, the basis set used is 6-31G\* for H, C, N, and O and VTZ, TZVP, or Lanl2DZ for Fe. For selected functionals, a diffuse function 6-31+G\* was added to N and O to better allow for molecular polarity and possible partial charge on the donor atoms. For the combination of the VTZ and TZVP basis sets on iron with the B3LYP and M062X functionals, strong spin contamination (0.87 for B3LYP and 0.95 for M062X) prevented, in some cases, the calculation of stable electronic structures.

As shown in Table 1, the BP86, mPW91, and PBE1PBE functionals, regardless of basis set, underestimate the Fe–NO bond length by up to 3.5 pm. The B3LYP, M06L, and  $\omega$ B97X-D functionals reproduce the experimentally observed values quite accurately, while the M062X grossly overestimates the Fe–NO bond length. The basis set effect on this parameter is negligible. For the N–O bond length, the majority of the calculations with a variety of basis sets overestimate this parameter, but the accuracy is better than for the Fe–NO bond length. Interestingly, the basis set effect here is much higher, with the Lanl2DZ basis set on all atoms performing poorly compared to other methods. This can be rationalized by the iron back-donation to the N–O  $\pi^*$  orbital because this would make the Fe–NO bond short and elongate the N–O bond.

All functional/basis set combinations predict the Fe–N–O angle within 4° except for M062X, which gives a value 17° higher than the experimental value of 142.7°. The better of the predictions seem to occur in basis sets with simplified electronic systems such as the VTZ basis with no polarization function and Lanl2DZ with core effective potentials shown in Table 2 (BP86/VTZ, B3LYP/Lanl2dz, M06L/Lanl2dz).

An important feature of  $[\text{Fe}(\text{OEP})(\text{NO})]$  that has been observed by the Scheidt group<sup>14b</sup> is the different bond lengths of the four equatorial Fe–N bonds. Two short Fe–Np distances are in the direction of the tilted NO ligand, while two long Fe–Np distances are opposite the off-axis NO tilt. This anisotropic effect can be simplified to the different bond lengths of two short patterns and two long patterns, as shown in Table 1. All functional/basis set combinations except the M062X method predict this feature well. The observed difference of  $N_{\text{p-long}} - N_{\text{p-short}}$  was 2.1 pm in the crystal structure and ranged from 1.0 to 3.0 pm in calculations.

In summary, the M062X functional provides poor results for several of the geometric parameters, namely, the Fe–NO distance and the Fe–N–O angle, and cannot therefore be recommended for the systems under study here. Both of the GGA functionals, BP86 and mPWPW91, perform better but still underestimate the Fe–NO bond by about 3.5 pm and overestimate the N–O bond by about 2.5 pm. Better predictions were obtained from the B3LYP, M06L, and  $\omega$ B97X-D functionals with a suitable basis set, all having agreement with experimental data within 1.0 pm for both bonds. M06L clearly stands out as providing the best agreement with experimental results.

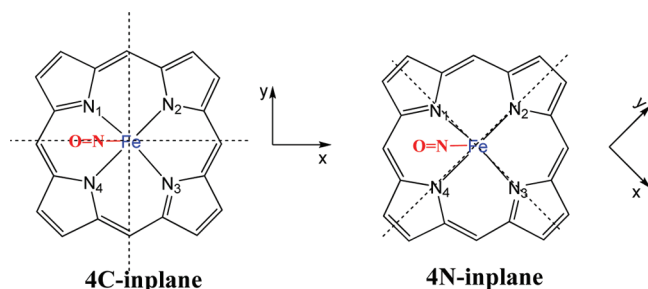
#### Fe–NO Stretch and Fe–N–O Bending Vibrational Modes.

The Fe–NO stretch and Fe–N–O bending modes are two major vibrations in  $[\text{Fe}(\text{OEP})(\text{NO})]$  that have high frequencies and strong intensities. In the Fe–N–O bending mode, the motions of Fe and O are in the same direction and opposite to the nitrosyl nitrogen, while the Fe–NO stretch mode was predicted to have the opposite direction motion between the Fe and NO groups (Figure 2). Both the Fe–NO stretching and Fe–N–O bending frequencies are listed in Table 2 with the functional method and basis set designated.

As shown in Table 2, the GGA functionals, BP86 and mPWPW91, severely overestimate the Fe–NO stretching frequency ( $>615 \text{ cm}^{-1}$  predicted vs  $517 \text{ cm}^{-1}$  observed). This difference is too large to be explained with anharmonicity and is likely because the Fe–NO bond lengths are underestimated. The other methods, including the hybrid-GGA, meta-GGA, and long-range GGA, provide better prediction for the stretch mode ranging from  $448 \text{ cm}^{-1}$  to  $551 \text{ cm}^{-1}$ . The exact frequency of  $517 \text{ cm}^{-1}$  was predicted by the B3LYP and M06L methods with the 6-31G\*/lanl2dz basis set. The PBE1PBE, LC-BP86, and  $\omega$ B97X-D were significantly less accurate than B3LYP and M06L. All of the Fe–N–O bending mode predictions are within  $50 \text{ cm}^{-1}$  of the experiment observation. The M06L method predicts it accurately to within  $2\text{--}3 \text{ cm}^{-1}$  when the VTZ basis set for Fe was used. Although the BP86 and mPWPW91 provides the Fe–N–O angle closer to the experimental value, it does not give a better bending frequency prediction. It is clear that the harmonic approximation common to all calculations leads to deviations from the experimentally observed values but that the computed values still allow a clear assignment of the normal modes.

**Prediction of Powder NRVS of  $[\text{Fe}(\text{OEP})(\text{NO})]$ .** The main goal of this work was to determine the best practices for the prediction of NRVS. To investigate the effects of DFT methods and basis sets, we calculated the NRVS powder spectrum of  $[\text{Fe}(\text{OEP})(\text{NO})]$ . This spectrum has all of the vibrational modes of iron including the Fe–NO stretch mode and Fe–N–O bending modes discussed earlier. Selected NRVS predicted spectra are shown in Figure 3, and predicted spectra using other functionals can be found in the

**Scheme 2. The Possible Orientations of Interest in Porphyrin Plane**



**Supporting Information.** As can be seen in Figure 3, the NRVS can conveniently be divided into three frequency domains for which the mode assignment has been discussed in detail previously.<sup>12b,30</sup> Here, we will discuss the performance of the different methods in terms of the different frequency domains.

In the region  $>360 \text{ cm}^{-1}$ , there are two important modes (Fe–NO stretch and Fe–N–O bend) in the observed NRVS spectrum and in each predicted spectrum (Figure 3A–F). There is an additional or partial peak in the  $>360 \text{ cm}^{-1}$  region when the long-range LC-BP86 method was used (Figure 3C). It could be an overestimated mode from the  $220\text{--}360 \text{ cm}^{-1}$  region. However, M06L was the best of the methods and was chosen to investigate the effects of the basis sets at the NRVS level (Figure 3D–F). As seen in Figure 3D and E, increasing the basis function from 6 to 31G\* to 6-31+G\* can move the Fe–NO stretch, and it is somewhat underestimated. In Figure 3D, the bending mode and stretch mode had shifted from 398 and 496 to 392 and 481, respectively. Similar trends can be seen in Figure 3E. The VTZ and TZVP basis sets show little difference. However, the Lanl2DZ basis set gives inconsistent frequency predictions (Figure 3F).

In the region  $220\text{--}360 \text{ cm}^{-1}$ , the two high-intensity peaks are observed with considerable spectral crowding. Most mode frequencies are poorly predicted by all functionals except M06L. The worst predictions are obtained by using GGA functionals with three apparently independent peaks (Figure 3A). The largely overestimated spectra are predicted with the long-range GGA functionals. As shown in Figure 3C, the major peaks move to the high-frequency region and are far away from the experimental observation designated by the black line. The better spectra are generated by the M06L functional with suitable basis set combinations. The spectra are almost coincident with the experimental spectra when the VTZ or TZVP basis set for Fe is used in the calculation (Figure 3D and E). However, the M06L functional is not quite as good when the Lanl2DZ basis set is used (Figure 3F).

All of the calculations gave similar spectral predictions in the  $<220 \text{ cm}^{-1}$  region where the important doming mode occurs. However, all DFT methods used here underestimate the doming mode frequency and overestimate its intensity. The results of the calculations should therefore be interpreted with caution.

**The In-Plane and Out-Plane NRVS of Single-Crystal  $[\text{Fe}(\text{OEP})(\text{NO})]$ .** Comparisons of DFT predictions to powder measurements do not account for the directional character of modes—that is substantial. A more detailed comparison needs to be done to capture the directional anisotropy. In porphyrin chemistry, analysis confined to the averaged porphyrin plane is usually defined as in-plane, and two directions are defined (in-plane  $x$  and in-plane  $y$ ). The third direction is

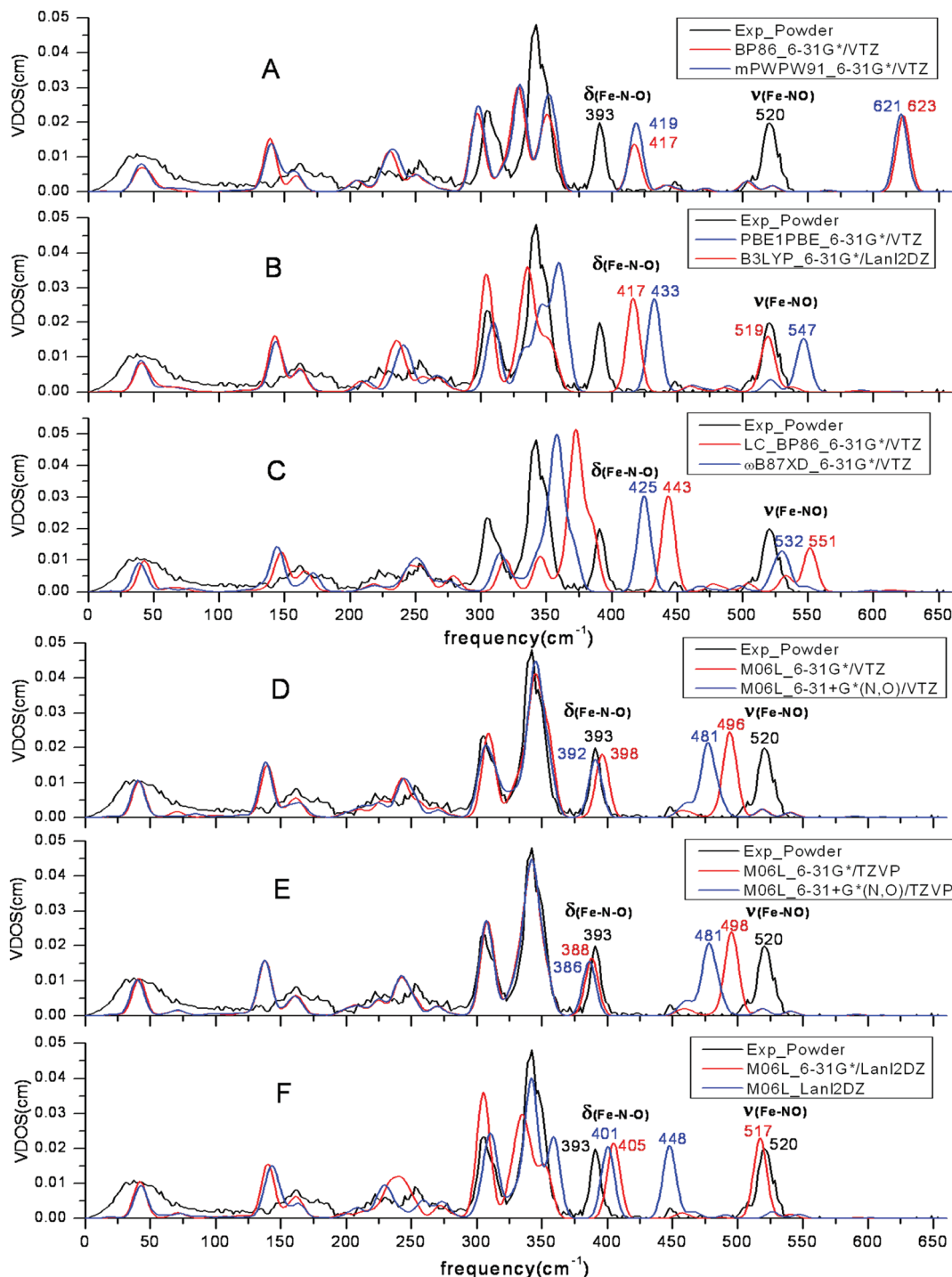


**Figure 3.** NRVS spectra of  $[\text{Fe(OEP)}(\text{NO})]$  with a variety of methods and basis sets with  $12 \text{ cm}^{-1}$  fwhh. The experimental observation of  $[\text{Fe(OEP)}(\text{NO})]$  powder is colored black, and the prediction data are colored red or blue (the same color strategy and fwhh in Figures 4–6).

perpendicular to the porphyrin plane and defined as out-of plane or the  $z$  direction. In this paper, in-plane  $x$  is parallel to the Fe–NO plane and  $y$  is perpendicular to the Fe–NO plane, as shown in Scheme 2. This axis selection is called 4C-inplane. Only functionals that predicted the powder spectrum well are used in the comparisons of  $x$ – $y$ – $z$ -directional spectra (Figure 4–6). The published data with the BP86 method were chosen to highlight the superiority of the M06L functional. The orientation-selective spectra using

other functionals can also be found in the Supporting Information.

The possible anisotropy in the in-plane NRVS spectrum can be shown by a measurement in two orthogonal in-plane directions. Conveniently, we chose, for measurements and predictions,  $x$  to be along the projection of the FeNO plane and  $y$  to be orthogonal. These are shown in Figures 4 and 5, respectively. As shown in Figure 4, there are three observed peaks in the  $>300 \text{ cm}^{-1}$  region, including one doublet peak at  $300\text{--}325 \text{ cm}^{-1}$ .

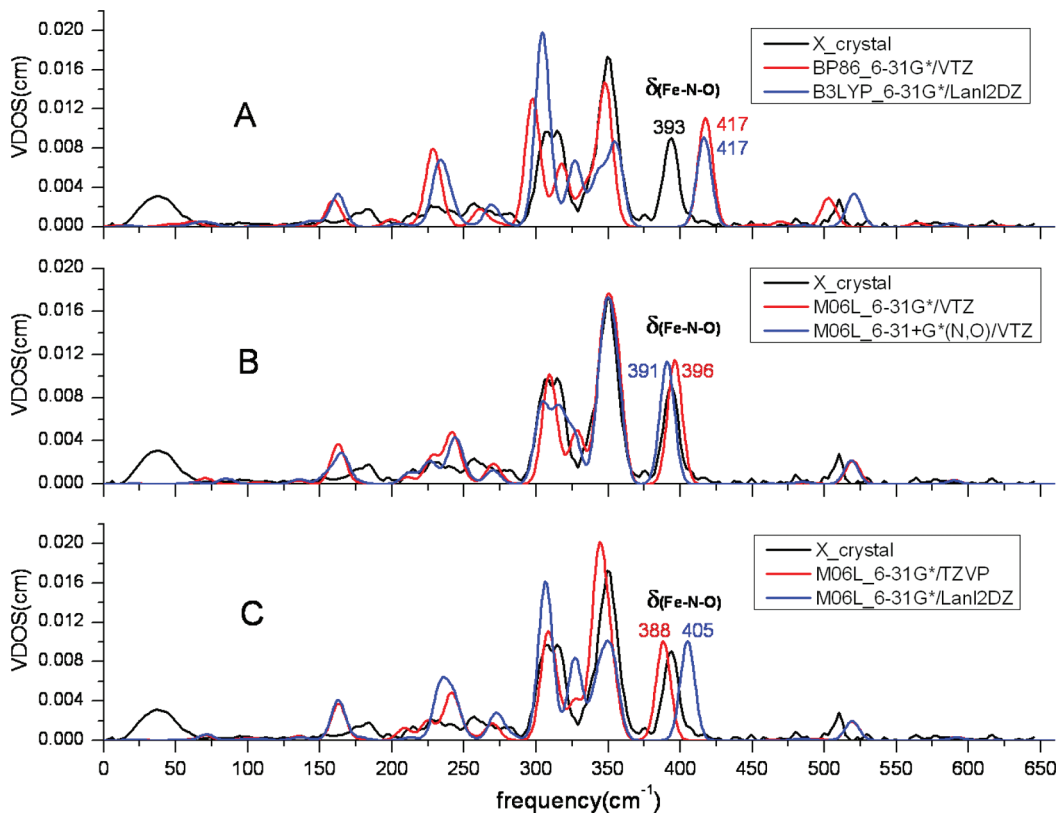


**Figure 4.** NRVS spectra of  $[\text{Fe}(\text{OEP})(\text{NO})]$  with selected methods and basis sets in the  $x$  direction, which is parallel to the intersection of porphyrin and  $\text{Fe}-\text{N}-\text{O}$  plane.

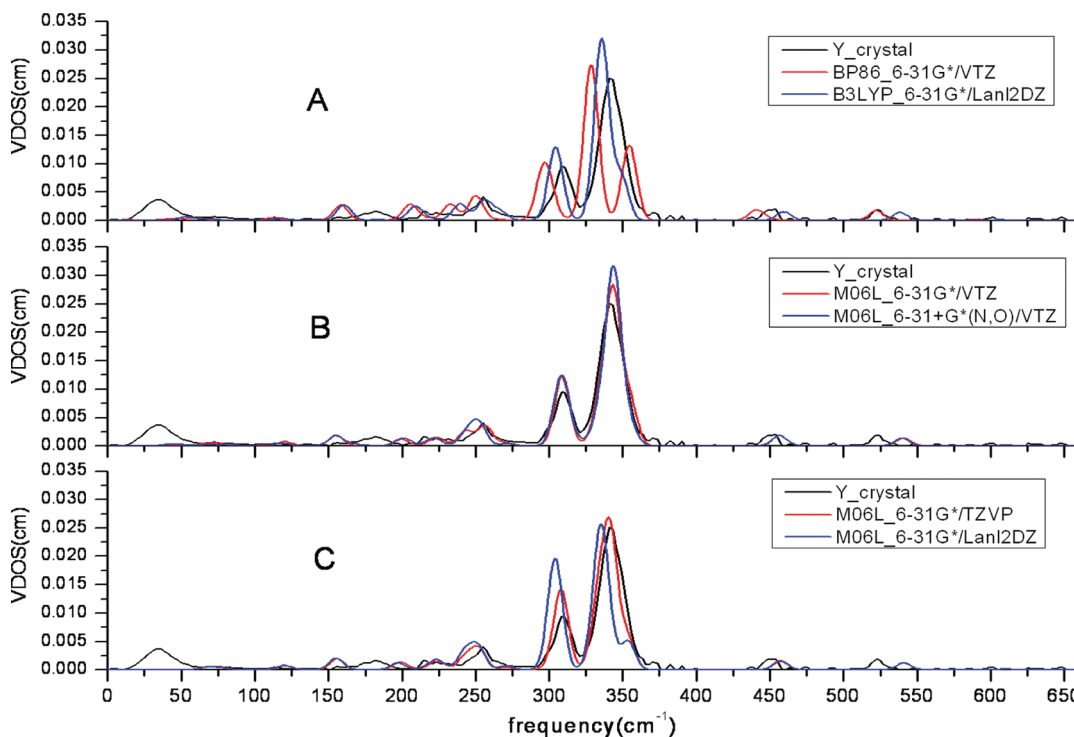


**Figure 5.** NRVS spectra of  $[\text{Fe}(\text{OEP})(\text{NO})]$  with selected methods and basis sets in the  $y$  direction, which is perpendicular to the  $\text{Fe}-\text{N}-\text{O}$  plane.

The observed doublet peak is only accurately predicted with the diffused function  $6-31+\text{G}^*$  for N and O (Figure 4B). The Lanl2DZ

basis set is unfavorable in the prediction of the NRVS spectrum, because more peaks are predicted from  $300 \text{ cm}^{-1}$  to  $360 \text{ cm}^{-1}$

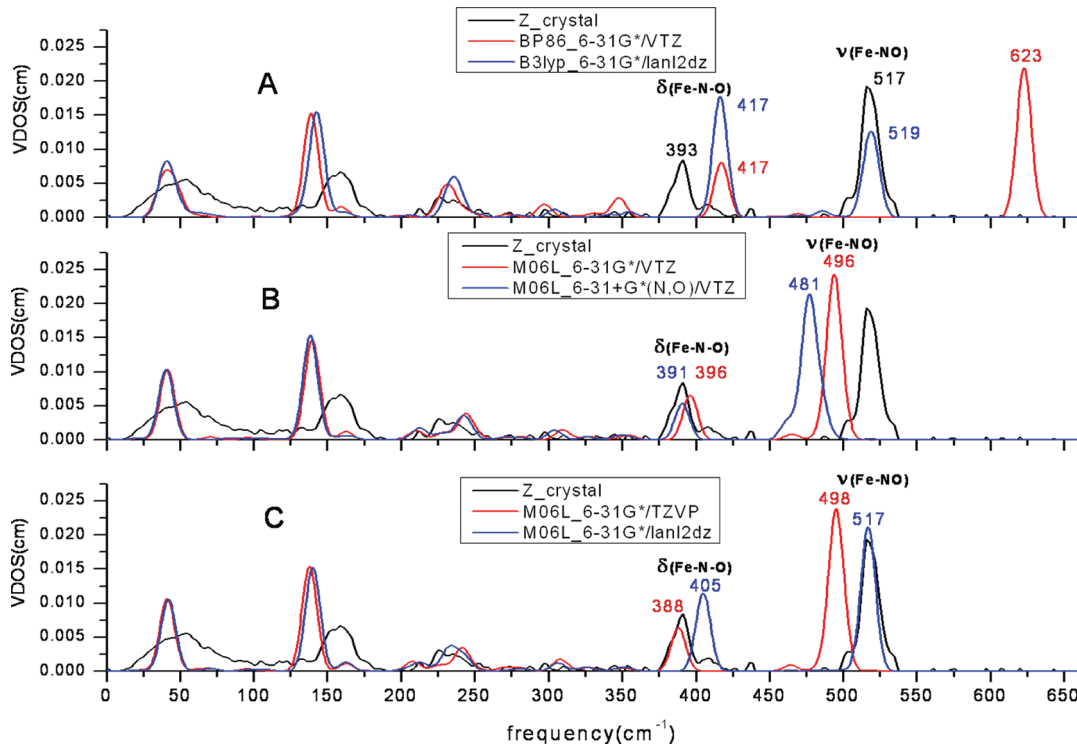


**Figure 6.** NRVS spectra of  $[\text{Fe}(\text{OEP})(\text{NO})]$  with selected methods and basis sets in the  $z$  direction, which is perpendicular to the average porphyrin plane.

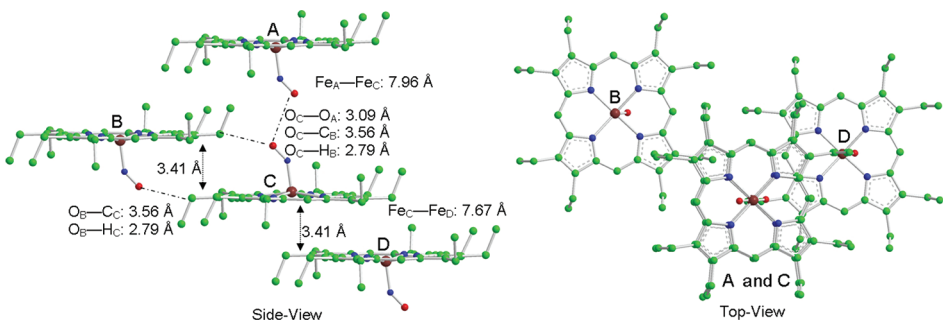


**Figure 7.** Crystal structures of triclinic  $[\text{Fe}(\text{OEP})(\text{NO})]$ . Hydrogen atoms have been omitted for clarity. Atom color: Fe (dark red), N (blue), O (red), C (green).

than observed and the bending mode around  $390 \text{ cm}^{-1}$  in the  $x$  direction is overestimated in both cases (Figure 4A/blue line and C/blue line). In sharp contrast, all of the major peaks in the NRVS along the  $y$  direction were underestimated when Lanl2DZ was used (Figure 5A/blue line and C/blue line). The BP86 functional is ruled out because three peaks are predicted, and only two are observed (Figure 5A). M06L with the VTZ or TZVP basis set shows better prediction than all others not only along the  $x$  direction but also along the  $y$  direction of NRVS.

The predictions of the out-of-plane NRVS spectra, shown in Figure 6, do not agree as well with experimental data as the in-plane spectra. The predicted doming modes are around  $140 \text{ cm}^{-1}$  regardless of the functional and basis set used, while the experimental observation is a broad peak at  $160 \text{ cm}^{-1}$ . The bending mode in the  $z$ -direction component is better predicted only when the M06L and VTZ basis sets were used, as shown in

Figure 6B. It is surprising that the stretch mode was perfectly predicted by the DFT calculation with the Lanl2DZ basis set, which in general gave poor predictions, as discussed above (Figure 6A and C). This presents a dilemma when using the Lanl2DZ basis set, because it predicts the stretch mode perfectly but fails on others modes. The diffuse function is not suitable for the prediction of the stretch mode, and it underestimates the experimental observations (Figure 6B). It is also inconsistent with the basis set strategy for in-plane NRVS.

A probable explanation is the difference between the gas-phase calculation and solid-state experiment. The predicted model is a single molecule without any intermolecular interactions, while both the experimental powder and crystal are in a crystal lattice and have intermolecular interactions or cooperativity. Figure 7 presents some likely intermolecular interactions. The distance between crystal layers is  $3.41 \text{ \AA}$ , and the closest distance between two irons is  $7.67 \text{ \AA}$ . This suggest that an intrinsic interaction

between different crystal layers could affect the out-of-plane modes more than in-plane ones. For the in-plane modes, the intermolecular close contacts cannot easily influence the iron center due to long distances. Therefore, the in-plane NRVS spectra may be more easily modeled. These unaccounted for forces can also explain why the out-of-plane spectra are always more difficult to predict accurately. The perfectly predicted stretching frequency by Lanl2DZ is probably the result of chance rather than ideal modeling and basis set because it fails to predict other modes.

## CONCLUSIONS

It is important to validate density functional methods in order to accurately predict directional anisotropy, a new feature in nuclear resonance vibrational spectroscopy (NRVS),<sup>12b</sup> and to reliably assign the vibrational modes. The scripts discussed here and made available in the Supporting Information allow the facile calculation of orientation-selective mode composition factors ( $e^2$ ), vibrational densities of states (VDOS), and NRVS data from standard Gaussian outputs. The extensive benchmarking of 21 different electronic structure methods for the representative case of the [Fe(OEP)NO] complex indicates that the M06L functional with suitable basis sets such as VTZ/6-31+G\* or TZVP/6-31+G\* provides the best agreement between calculated and experimental structures and NRVS data, followed by the B3LYP/6-31G\*/LanL2DZ method. This is presumably due to the accurate description of the open-shell system and accurate excitation energies,<sup>31</sup> which are likely to be important due to the low lying excited states in heme complexes, by the M06L functional.

A comparison of computational NRVS predictions and experimental data reveals that the M06L functional shows excellent agreement in the frequency domains of  $>360\text{ cm}^{-1}$  and  $200\text{--}360\text{ cm}^{-1}$ . However, the frequencies of the modes in the region below  $200\text{ cm}^{-1}$  are underestimated by all methods, including the M06L functional. A more detailed analysis of the anisotropic NRVS data shows that the M06L functional gives very good results for in-plane ( $x$  and  $y$ ) but less so for out-of-plane ( $z$ ) NRVS. The prediction of the in-plane NRVS using the M06L functional still exhibits the best performance, while the out-of-plane vibrations are less well predicted. This is most likely due to limitations of the model, which does not consider the crystal packing contacts that more influence the out-of-plane but not the in-plane vibrations.

In summary, the protocol presented here allows the facile and accurate prediction of NRVS data for the purpose of making assignments and to understand the detailed geometric and electronic structure of heme complexes.

## ASSOCIATED CONTENT

**Supporting Information.** Perl scripts, procedure for using the scripts, and  $e^2$  values and computed NRVS spectra in three orthogonal directions as well as Cartesian coordinates and total energies of all structures discussed. This material is available free of charge via the Internet at <http://pubs.acs.org>

## AUTHOR INFORMATION

### Corresponding Author

\*Tel.: +5746315876. Fax: +5746316652. E-mail: owiest@nd.edu.

### Notes

The authors declare no competing financial interest.

## ACKNOWLEDGMENT

We gratefully acknowledge support of this research by the National Institutes of Health (Grant GM-38401 to W.R.S.). Generous allocation of computing resources by the Center for Research Computing at the University of Notre Dame and by the National Science Foundation through TeraGrid resources under grant number TG-CHE090124 are also acknowledged.

## REFERENCES

- (a) Berezin, B. D. *Coordination Compounds of Porphyrins and Phthalocyanines*; John Wiley & Sons Ltd.: New York, 1981; pp 1–10. (b) *Iron Porphyrins*; Lever, A. B. P., Gray, H. B., Eds.; Addison-Wesley Publishing Company Inc.: Reading, MA, 1983; pp 1–274.
- (2) Richter-Addo, G. B.; Legzdins, P.; Burstyn, J. *Chem. Rev.* **2002**, *102*, 857.
- (3) (a) Yu, A. E.; Hu, S.; Spiro, T. G.; Burstyn, J. N. *J. Am. Chem. Soc.* **1994**, *116*, 4117. (b) Negrierie, M.; Kruglik, S. G.; Lambry, J.; Vos, M. H.; Martin, J.; Franzen, S. *J. Biol. Chem.* **2006**, *281*, 10389.
- (4) Vogel, K. M.; Kozlowski, P. M.; Zgierski, M. Z.; Spiro, T. G. *Inorg. Chim. Acta* **2000**, *297*, 11.
- (5) Leu, B. M.; Zgierski, M. Z.; Wyllie, G. R. A.; Scheidt, W. R.; Sturhahn, W.; Alp, E. E.; Durbin, S. M.; Sage, J. T. *J. Am. Chem. Soc.* **2004**, *126*, 4211.
- (6) Scheidt, W. R.; Dubin, S. M.; Sage, J. T. *J. Inorg. Biochem.* **2005**, *99*, 60.
- (7) (a) Xiao, Y.; Wang, H.; George, S. J.; Smith, M. C.; Adams, M. W.; Jenney, F. E.; Sturhahn, W., Jr.; Alp, E. E.; Zhao, J.; Yoda, Y.; Dey, A.; Solomon, E. I.; Cramer, S. P. *J. Am. Chem. Soc.* **2005**, *127*, 14596. (b) Leu, B. M.; Zgierski, M. Z.; Wyllie, G. R.; Scheidt, W. R.; Sturhahn, W.; Alp, E. E.; Durbin, S. M.; Sage, J. T. *J. Am. Chem. Soc.* **2004**, *126*, 4211. (c) Achterhold, K.; Sturhahn, W.; Alp, E. E.; Parak, F. G. *Hyperfine Interact.* **2002**, *141*–142. (d) Xiao, Y.; Tan, M. L.; Ichijo, T.; Wang, H.; Guo, Y.; Smith, M. C.; Meyer, J.; Sturhahn, W.; Alp, E. E.; Zhao, J.; Yoda, Y.; Cramer, S. P. *Biochemistry* **2008**, *47*, 6612. (e) Xiao, Y.; Fisher, K.; Smith, M. C.; Newton, W. E.; Case, D. A.; George, S. J.; Wang, H.; Sturhahn, W.; Alp, E. E.; Zhao, J.; Yoda, Y.; Cramer, S. P. *J. Am. Chem. Soc.* **2006**, *128*, 7608. (f) Rai, B. K.; Durbin, S. M.; Prohofsky, E. W.; Sage, J. T.; Wyllie, G. R.; Scheidt, W. R.; Sturhahn, W.; Alp, E. E. *Biophys. J.* **2002**, *82*, 2951. (g) Rai, B. K.; Durbin, S. M.; Prohofsky, E. W.; Sage, J. T.; Ellison, M. K.; Roth, A.; Scheidt, W. R.; Sturhahn, W.; Alp, E. E. *J. Am. Chem. Soc.* **2003**, *125*, 6927. (h) Rai, B. K.; Prohofsky, E. W.; Durbin, S. M. *J. Phys. Chem. B* **2005**, *109*, 18983. (h) Cramer, S.; Xiao, Y.; Wang, H.; Guo, Y.; Smith, M. *Hyperfine Interact.* **2007**, *170*, 47. (i) Petrenko, T.; DeBeer, S.; Aliaga-Alcalde, George, N.; Bill, E.; Mienert, B.; Xiao, Y.; Guo, Y.; Sturhahn, W.; Cramer, S. P.; Wieghardt, K.; Neese, F. *J. Am. Chem. Soc.* **2007**, *129*, 11053.
- (8) (a) Paulsen, H.; Winkler, H.; Trautwein, A. X.; Grünsteudel, H.; Rusanov, V.; Toftlund, H. *Phys. Rev. B* **1999**, *59*, 975. (b) Paulsen, H.; Benda, R.; Herta, C.; Schünemann, V.; Chumakov, A. I.; Duelund, L.; Winkler, H.; Toftlund, H.; Trautwein, A. X. *Phys. Rev. Lett.* **2001**, *86*, 1351. (c) Paulsen, H.; Rusanov, V.; Benda, R.; Herta, C.; Schünemann, V.; Janiak, C.; Dorn, T.; Chumakov, A. I.; Winkler, H.; Trautwein, A. X. *J. Am. Chem. Soc.* **2002**, *124*, 3007. (d) Sandala, G. M.; Hopmann, K. H.; Ghosh, A.; Noddleman, L. *J. Chem. Theory Comput.* **2011**, *7*, 3232.
- (9) (a) Zhou, M.; Andrews, L.; Bauschlicher, C. W., Jr. *Chem. Rev.* **2001**, *101*, 1931. (b) Ghosh, A.; Bocian, D. F. *J. Phys. Chem.* **1996**, *100*, 6363. (c) Kozlowski, P. M.; Jarzecki, A. A.; Pulay, P.; Li, X.-Y.; Zgierski, M. Z. *J. Phys. Chem.* **1996**, *100*, 13985. (d) Kozlowski, P. M.; Spiro, T. G.; Bérces, A.; Zgierski, M. Z. *J. Phys. Chem. B* **1998**, *102*, 2603. (e) Ghosh, A.; Skancke, A. *J. Phys. Chem. B* **1998**, *102*, 10087. (f) Kozlowski, P. M.; Spiro, T. G.; Zgierski, M. Z. *J. Phys. Chem. B* **2000**, *104*, 10659. (g) Cao, Z.; Hall, M. B. *J. Am. Chem. Soc.* **2001**, *123*, 3734. (h) Franzen, S. *J. Am. Chem. Soc.* **2001**, *123*, 12578. (i) Steene, E.; Wondimagegn, T.; Ghosh, A. *J. Inorg. Biochem.* **2002**, *88*, 113. (j) Ohta, T.; Matsuura, K.; Yoshizawa, K.; Morishima, I. *J. Inorg. Biochem.* **2000**, *82*, 141. (k) Maréchal, J.-D.; Maseras, F.; Lledós, A.; Mouawad, L.;

- Perahia, D. *Chem. Phys. Lett.* **2002**, *353*, 379. (l) Liao, M.-S.; Scheiner, S. *J. Chem. Phys.* **2002**, *116*, 3635.
- (10) For selected papers: (a) Praneeth, V. K. K.; Neather, C.; Peters, G.; Lehnert, N. *Inorg. Chem.* **2006**, *45*, 2795. (b) Paulat, F.; Berto, T. C.; DeBeer George, S.; Goodrich, L.; Praneeth, V. K. K.; Sulok, C. D.; Lehnert, N. *Inorg. Chem.* **2008**, *47*, 11449. (c) Berto, T. C.; Praneeth, V. K. K.; Goodrich, L.; Lehnert, N. *J. Am. Chem. Soc.* **2009**, *131*, 17116. (d) Lehnert, N.; Galinato, M. G.; Paulat, F.; Richter-Addo, G. B.; Sturhahn, W.; Xu, N.; Zhao, J. *Inorg. Chem.* **2010**, *49*, 4133.
- (11) Oxaard, J.; Wiest, O. *J. Phys. Chem. A* **2001**, *105*, 8236.
- (12) (a) Scheidt, W. R.; Barabanschikov, A.; Pavlik, J. W.; Silvernail, N. J.; Sage, J. T. *Inorg. Chem.* **2010**, *49*, 6240. (b) Pavlik, J. W.; Barabanschikov, A.; Oliver, A. G.; Alp, E. E.; Sturhahn, W.; Zhao, J.; Sage, J. T.; Scheidt, W. R. *Angew. Chem., Int. Ed.* **2010**, *49*, 4400.
- (13) Ghosh, A. *J. Biol. Inorg. Chem.* **2006**, *11*, 712.
- (14) (a) Ellison, M. K.; Scheidt, W. R. *J. Am. Chem. Soc.* **1997**, *119*, 7404. (b) Scheidt, W. R.; Duval, H. F.; Neal, T. J.; Ellison, M. K. *J. Am. Chem. Soc.* **2000**, *122*, 4651.
- (15) (a) Patchkovskii, S.; Ziegler, T. *Inorg. Chem.* **2000**, *39*, 5354. (b) Silvernail, N. J.; Barabanschikov, A.; Sage, J. T.; Noll, B. C.; Scheidt, W. R. *J. Am. Chem. Soc.* **2009**, *131*, 2131.
- (16) (a) Silvernail, N. J.; Pavlik, J. W.; Noll, B. C.; Schulz, C. E.; Scheidt, W. R. *Inorg. Chem.* **2008**, *47*, 912. (b) Silvernail, N. J.; Olmstead, M. M.; Noll, B. C.; Scheidt, W. R. *Inorg. Chem.* **2009**, *48*, 971.
- (17) Frisch, M. J.; Trucks, G. W.; Schlegel, H. B.; Scuseria, G. E.; Robb, M. A.; Cheeseman, J. R.; Scalmani, G.; Barone, V.; Mennucci, B.; Petersson, G. A.; Nakatsuji, H.; Caricato, M.; Li, X.; Hratchian, H. P.; Izmaylov, A. F.; Bloino, J.; Zheng, G.; Sonnenberg, J. L.; Hada, M.; Ehara, M.; Toyota, K.; Fukuda, R.; Hasegawa, J.; Ishida, M.; Nakajima, T.; Honda, Y.; Kitao, O.; Nakai, H.; Vreven, T.; Montgomery, J. A., Jr.; Peralta, J. E.; Ogliaro, F.; Bearpark, M.; Heyd, J. J.; Brothers, E.; Kudin, K. N.; Staroverov, V. N.; Kobayashi, R.; Normand, J.; Raghavachari, K.; Rendell, A.; Burant, J. C.; Iyengar, S. S.; Tomasi, J.; Cossi, M.; Rega, N.; Millam, J. M.; Klene, M.; Knox, J. E.; Cross, J. B.; Bakken, V.; Adamo, C.; Jaramillo, J.; Gomperts, R.; Stratmann, R. E.; Yazyev, O.; Austin, A. J.; Cammi, R.; Pomelli, C.; Ochterski, J. W.; Martin, R. L.; Morokuma, K.; Zakrzewski, V. G.; Voth, G. A.; Salvador, P.; Dannenberg, J. J.; Dapprich, S.; Daniels, A. D.; Farkas, O.; Foresman, J. B.; Ortiz, J. V.; Cioslowski, J.; Fox, D. J. *Gaussian 09*, Revision A.02; Gaussian, Inc.: Wallingford, CT, 2009.
- (18) Achterhold, K.; Keppler, C.; Ostermann, A.; Burck, U.; Sturhahn, W.; Alp, E. E.; Parak, F. G. *Phys. Rev.* **2002**, *E65*, 051916.
- (19) Merrick, J. P.; Moran, D.; Radom, L. *J. Phys. Chem. A* **2007**, *111*, 11683.
- (20) (a) Becke, A. D. *Phys. Rev.* **1988**, *A38*, 3098. (b) Perdew, J. P. *Phys. Rev. B* **1986**, *33*, 8822.
- (21) (a) Adamo, C.; Barone, V. *J. Chem. Phys.* **1998**, *108*, 664. (b) Perdew, J. P.; Chevary, J. A.; Vosko, S. H.; Jackson, K. A.; Pederson, M. R.; Singh, D. J.; Fiolhais, C. *Phys. Rev. B* **1992**, *46*, 6671.
- (22) (a) Becke, A. D. *Phys. Rev.* **1988**, *A38*, 3098. (b) Becke, A. D. *J. Chem. Phys.* **1993**, *98*, 1372. (c) Becke, A. D. *J. Chem. Phys.* **1993**, *98*, 5648. (d) Lee, C.; Yang, W.; Parr, R. G. *Phys. Rev.* **1988**, *B37*, 785.
- (23) (a) Perdew, J. P.; Burke, K.; Ernzerhof, M. *Phys. Rev. Lett.* **1996**, *77*, 3865. (b) Perdew, J. P.; Burke, K.; Ernzerhof, M. *Phys. Rev. Lett.* **1997**, *78*, 1396.
- (24) Zhao, Y.; Truhlar, D. G. *Theor. Chem. Acc.* **2008**, *120*, 215.
- (25) Zhao, Y.; Truhlar, D. G. *J. Chem. Phys.* **2006**, *125*, 194101: 1.
- (26) Iikura, H.; Tsuneda, T.; Yanai, T.; Hirao, K. *J. Chem. Phys.* **2001**, *115*, 3540.
- (27) Chai, J.-D.; Head-Gordon, M. *Phys. Chem. Chem. Phys.* **2008**, *10*, 6615.
- (28) The basis sets can be found in the following references: (a) Hay, P. J.; Wadt, W. R. *J. Chem. Phys.* **1985**, *82*, 270–283; *ibid.*, *82*, 299. (b) Wadt, W. R.; Hay, P. J. *J. Chem. Phys.* **1985**, *82*, 284. (c) Schafer, A.; Horn, H.; Ahlrichs, R. *J. J. Phys. Chem.* **1992**, *97*, 2571. (d) Schafer, A.; Huber, C.; Ahlrichs, R. *J. Chem. Phys.* **1994**, *100*, 5829.
- (29) Sage, J. T.; Paxson, C.; Wyllie, G. R. A.; Sturhahn, W.; Durbin, S. M.; Champion, P. M.; Alp, E. E.; Scheidt, W. R. *J. Phys.: Condens. Matter* **2001**, *13*, 7707.
- (30) Li, J. F.; Peng, Q.; Barabanschikov, A.; Pavlik, J. W.; Alp, E. E.; Sturhahn, W.; Zhao, J.; Schulz, C. E.; Sage, J. T.; Scheidt, W. R. *Chem.—Eur. J.* **2011**, *17*, 11178.
- (31) Jacquemin, D.; Prepette, E. A.; Ciofini, I.; Adamo, C.; Valero, R.; Zhao, Y.; Truhlar, D. G. *J. Chem. Theory Comput.* **2010**, *6*, 2071.